



Effect of stress and temperature on the micromechanics of creep in highly irradiated bone and dentin

Anjali Singhal ^{a,*}, Alix C. Deymier-Black ^a, Jonathan D. Almer ^b, David C. Dunand ^a

^a Department of Materials Science and Engineering, Northwestern University, Evanston, IL 60208, USA

^b X-ray Science Division, Advanced Photon Source, Argonne National Laboratory, Argonne, IL 60439, USA

ARTICLE INFO

Article history:

Received 30 April 2012

Received in revised form 12 August 2012

Accepted 14 December 2012

Available online 23 December 2012

Keywords:

Bone

Dentin

Creep

Irradiation

Synchrotron X-ray diffraction

Temperature

ABSTRACT

Synchrotron X-ray diffraction is used to study *in situ* the evolution of phase strains during compressive creep deformation in bovine bone and dentin for a range of compressive stresses and irradiation rates, at ambient and body temperatures. In all cases, compressive strains in the collagen phase increase with increasing creep time (and concomitant irradiation), reflecting macroscopic deformation of the sample. By contrast, compressive elastic strains in the hydroxyapatite (HAP) phase, created upon initial application of compressive load on the sample, decrease with increasing time (and irradiation) for all conditions; this load shedding behavior is consistent with damage at the HAP–collagen interface due to the high irradiation doses (from ~100 to ~9,000 kGy). Both the HAP and fibril strain rates increase with applied compressive stress, temperature and irradiation rate, which is indicative of greater collagen molecular sliding at the HAP–collagen interface and greater intermolecular sliding (i.e., plastic deformation) within the collagen network. The temperature sensitivity confirms that testing at body temperature, rather than ambient temperature, is necessary to assess the *in vivo* behavior of bone and teeth. The characteristic pattern of HAP strain evolution with time differs quantitatively between bone and dentin, and may reflect their different structural organization.

© 2013 Elsevier B.V. All rights reserved.

1. Introduction

Hard bio-mineralized tissues such as bone and dentin have a complex, hierarchically organized structure. Although structurally different, in mammals both of these materials are composed of the same components: a mineral phase (calcium hydroxyapatite, HAP), a protein phase (mostly type-I collagen), and fluid phases (water, saliva, or blood) [1,2]. Through a unique assembly of these phases, bone and dentin exhibit a combination of high strength, high toughness, high wear-resistance (for teeth), and self-repair (for bone), enabling them to perform for years under physiological loads and at body temperature. There is strong evolutionary pressure to achieve optimized mechanical properties in these tissues, given that bones are the primary load-bearing structures of the body and that teeth enable feeding. The study of the mechanical properties of healthy bone and teeth is thus of interest, both fundamentally, and to provide a comparison with diseased or injured tissues. A thorough understanding of the mechanics of bone and teeth under long-term loading is also

of interest for the success of bone and tooth synthetic implants or replacement materials.

A number of studies have examined the elastic [3–10] and fracture properties [11–20] of bone and dentin of humans, bovines, equines and elephants which are relevant to rapid and transient loads. Less attention has been devoted to the time-dependent behavior of these tissues, which behave visco-elastically under long-term stresses. Although not the most common loading condition for bone and dentin, long terms stresses do occur due to muscular action or during treatments of conditions such as scoliosis [21], the use of rib-spreaders during thoracic surgery [22], and the use of orthodontic braces [23]. Rimnac et al. [24] have studied the effects of stress, temperature and microstructure on the macroscopic creep strains in bovine femur, and demonstrated, using semi-empirical models, that the creep rate is positively associated with the volume fraction of secondary Haversian bone, temperature and stress. Jantararat et al. [25] have shown a positive correlation ($r^2=0.79$) between the macroscopic creep rate of dentin and stress (from human canines and incisors). However, to truly understand the time-dependent behavior of bone and dentin it is necessary to determine the response of their individual phases in addition to the macroscopic behavior.

Combined X-ray wide- and small-angle scattering (WAXS/SAXS) is a technique through which the mechanical coupling between the mineral and protein phases can be assessed at the nanoscale via average strains measured in these two phases. WAXS/SAXS using high-energy ($E=70$ keV) synchrotron X-rays has been previously

* Corresponding author. Tel.: +1 773 290 9094(cell), +1 847 467 5416(work); fax: +1 847 491 7820.

E-mail addresses: anjalisinghal2007@u.northwestern.edu, anjali.singhal@gmail.com (A. Singhal), alixdeymier2010@u.northwestern.edu (A.C. Deymier-Black), almer@aps.anl.gov (J.D. Almer), dunand@northwestern.edu (D.C. Dunand).

used to determine the strains, *in situ* under an applied stress, in the individual phases of metal–matrix composites [26–30], and biological composites like fallow deer antler [31], canine bone [32,33], bovine bone [34–39] and bovine dentin [40–44]. Recently, we used this technique to explore creep deformation in bovine bone, but this study was limited to a single temperature (37 °C) and a single compressive stress (−80 MPa) [36]. In this study, the magnitude of the elastic strain in the HAP phase increases linearly with increasing creep time due to load transfer from the visco-elastically deforming collagen phase. This behavior is also observed in inorganic composites where the more compliant creeping matrix sheds load to the stiffer reinforcement (whose strain thus increases) via a strong interface, as the bulk deformation of the sample increases [45]. Thus, the mechanism associated with creep in bone and dentin appears to follow classical composite mechanics. However, in a subsequent study on creep of bone and dentin carried out at a single temperature (37 °C) and stress (−95 MPa) using the same technique, we observed that, under much higher irradiation doses, the magnitude of the compressive strain (and thus stress) carried by the HAP phase decreased with creep time, while the compressive strain in the fibrils increased with time [35]. This load shedding from the reinforcement to the matrix phase was assigned to damage of the HAP–collagen interface degrading the transfer of load from the matrix to the HAP platelets during creep [35].

In this study, we examine, for the first time in a systematic manner, the effect of the applied stress and temperature, on the mechanisms of load transfer between HAP and collagen during creep deformation of bovine bone and dentin which were subjected to high radiation doses. With the use of the synchrotron WAXS/SAXS technique, we investigate the effect of creep stresses in the range of −40 to −110 MPa on bovine bone and dentin at two different temperatures, 27 °C and 37 °C and a wide range of radiation doses (580–9400 kGy).

2. Experimental procedures

2.1. Sample preparation

Fresh bovine femurs of a healthy 18-month old Black Angus cow were obtained from Aurora Packing Company Inc. (North Aurora, IL), within 1 hour of slaughter. The preparation procedures are described in Ref. [39] but are summarized here. The femur was cleaned of marrow and any attached ligaments using scalpels. With an autopsy saw, the length of the femur was divided into 3 cylinders, each ~2 cm in height. The cylinders were then stored in gauze soaked with phosphate buffered saline (PBS) and frozen at −20 °C until further cutting. The total time elapsed between slaughter of the animal and freezing of cut sections was ~5 hours. Prior to cutting, one cylinder was thawed to room temperature. Transverse sections of the cylinder, 5 mm in height, were cut using a low-speed diamond wafering saw perpendicular to the femur long-axis. These transverse sections were further cut to obtain samples with sizes of $5.45 (\pm 0.01) \times 3.88 (\pm 0.01) \times 2.86 (\pm 0.01) \text{ mm}^3$. All cutting was done in deionized water to maintain the hydration state of the samples. Each sample was weighed on a precision balance three times, after blotting out the excess water from the surface. Their dimensions were measured three times with a point micrometer to calculate the volume. The density of the samples was calculated by taking a ratio of the average of the mass and volume measurements [46,47]. The samples were then stored in PBS and frozen at −20 °C until the time of the experiment.

Front incisors were extracted using dental pliers and scalpels from the lower mandible of another healthy 18-month old Black Angus cow obtained from Aurora Packing Company Inc., within an hour of death. The preparation of the samples, which has already been described in detail in Ref. [40], is summarized here. The extracted

teeth were stored in a mixture of PBS, 1% antibacterial and antifungal solution and frozen at −20 °C. The total time elapsed between slaughter of the animal and freezing of extracted teeth was ~5 hours. Prior to cutting, the teeth were thawed to room temperature. Parallel cuts, 8 mm apart, were made with a low-speed diamond wafering saw perpendicular to the tooth-growth direction. From each tooth, 1–2 cylindrical root dentin samples were obtained, 7.5 mm in height and with the natural cross-section of the tooth. The cutting was done in deionized water to prevent drying of the dentin. To calculate the apparent density, Archimedes tests were performed in water. Further, to determine the accurate cross-sectional area of the dentin cylinders, laboratory micro-CT was used [41]. The samples were stored in PBS and frozen at −20 °C until the time of the experiment.

2.2. X-ray scattering experiments

Mechanical testing with concurrent X-ray diffraction was performed at beamline 1-ID-C at the Advanced Photon Source, Argonne National Laboratory (Argonne, IL 60432). Bone and dentin samples were thawed to room temperature before testing. An MTS-858 load frame applied compressive load along the femur long-axis of the bone samples, and along the tooth growth direction of the dentin samples. A hydration rig made of vinyl tubing was attached to the lower platen to maintain the samples hydrated and at the appropriate temperature. Tests were carried out at 27 °C (room temperature) and 37 °C (body temperature). A schematic of the setup is shown in Fig. 1, and is similar to the setup used in previous works [36,39].

The bone and dentin samples were placed in the sample hydration rig such that the X-ray beam passed through their vertical and horizontal centers, determined using absorption measurements. For each experiment, an initial scattering measurement was taken at zero applied stress on a single sample, after which the sample was loaded in less than 10 seconds up to the desired stress level and maintained at a constant value for the rest of the experiment, lasting for 2–4 hours. Tests were done in two segments—high stresses ranging between −90 and −108 MPa and slightly lower stresses, ranging between −40 and −75 MPa. All the stresses used here are significantly higher than the stresses experienced in a physiological situation, which are in the range of 10–20 MPa as measured on a human femur and tibia [48,49], but similar to our previous work on creep in bone and dentin [35,36,44] where the main goal was to identify deformation mechanisms in the limited synchrotron beam time available.

In the first experimental segment, bone samples were tested at stresses of −95, −100 or −108 MPa at 27 (samples A–C) and 37 °C (samples J–L). Dentin samples were tested at −90 or −100 MPa at 27 °C (samples M–O), and −90 or −95 MPa at 37 °C (samples P–R). The sample treatment conditions along with their code names are listed in Table 1. A parallel X-ray beam with 65 keV energy and $50 \times 50 \mu\text{m}^2$ cross-section was used for these experiments. The results from the tests on bone and dentin samples at −95 MPa at 37 °C (samples J and R) have been reported in our earlier work [43], and are used here for comparison with the other stresses. Wide-angle X-ray scattering (WAXS) patterns for the HAP phase were recorded with a MAR 345 detector ($2,300 \times 2,300$ pixels, $150 \mu\text{m}^2/\text{pixel}$) which was placed at a distance of 1,269 mm from the sample. Small-angle X-ray scattering (SAXS) patterns for the collagen were recorded with a PI-CCD detector ($2,048 \times 2,048$ pixels, $80 \mu\text{m}^2/\text{pixel}$), placed at a distance of 4,000 mm from the sample. The exposure times for the WAXS and SAXS measurements were 50 and 30 seconds respectively, resulting in a total absorbed radiation dose of 24 kGy per WAXS + SAXS measurements, as indicated in Table 1. A total of 33 measurements were performed at regular time intervals on each sample over a time span of 2–3 hours, resulting in an accumulated

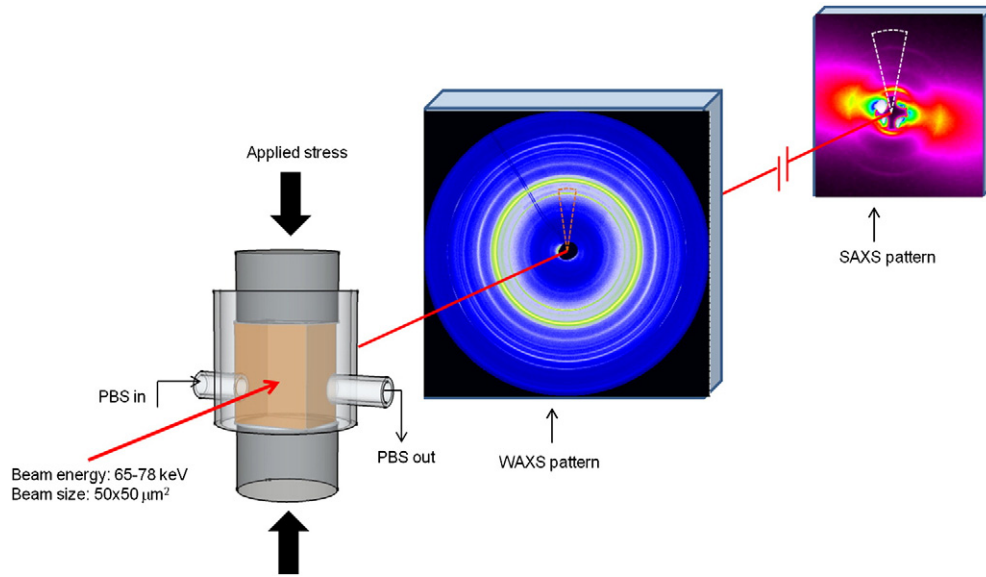


Fig. 1. Schematic of experimental setup for in situ synchrotron diffraction experiment at APS with experimental WAXS and SAXS patterns showing representative HAP and collagen fibrillar rings for bone sample K, respectively. The azimuthal angular ranges used for data analysis are indicated on each pattern by dashed arc-slices.

irradiation dose of 800 kGy over the span of the experimental time. All the samples in this experimental segment will be referred to as “low dose samples” in the text.

In a second experimental segment, only bone samples were tested at lower stresses of -40 , -55 and -75 MPa at 37°C (samples D–F) following the same loading routine as samples J–L. A second series of high stress experiments was also performed on bone samples (labeled G–I) at stresses of -95 , -100 and -105 MPa at 37°C . After 1 hour of creep at creep stress of -95 , -100 and -105 MPa, these samples G–I were unloaded to zero stress in -19 , -20 and -17 MPa decrements respectively, and immediately reloaded to their original creep stress in the same increments. The cycle of creep (for 1 hour), unloading and reloading was then repeated twice. In this work, the diffraction strain data collected during the unloading and reloading steps are not reported. These data are reported and discussed in our previous study on creep in bone and dentin [35]. Diffraction measurements were done with a 78 keV X-ray beam with a $50 \times 50 \mu\text{m}^2$ cross-section. The WAXS patterns were recorded with a MAR 165 detector (2048×2048 pixels, $80 \times 80 \mu\text{m}^2/\text{pixel}$), placed at a distance of 782 mm from the sample. The SAXS detector was the same as previously used. The WAXS and

SAXS exposure times were unchanged and resulted in a total absorbed dose of 78 kGy per WAXS + SAXS measurement and an accumulated dose of 7488 kGy over the 2–3 hour span of the experiment for samples D–F. The creep-unload samples (G–I) accumulated a slightly higher dose of 9400 kGy until the end of their ~4 hour experiment. All the samples tested in this second segment will be referred to as “high dose samples” in the following text. The total dose accumulated in the irradiated volumes up to the end of the experiment is also indicated in Table 1. The attenuation of the X-ray beam by the hydration rig and the PBS, before reaching the sample, is calculated to be 14% [50], and has not been taken into consideration for radiation dose calculations in Table 1.

2.3. Diffraction analysis

2.3.1. Strain measurement

The atomic-level periodicities in the HAP platelet diffract X-rays following Bragg's law, producing a WAXS diffraction pattern as shown in Fig. 1. The change in d-spacing within the platelet gives the elastic strain in the HAP phase. The regular arrangement of the HAP platelets within the collagen molecules results in periodic

Table 1
HAP volume content, apparent density, irradiation dose (per measurement and cumulative) and HAP and fibrillar strain rates during creep at the testing conditions.

Sample	Applied stress (MPa)	Temperature ($^\circ\text{C}$)	Radiation dose per measurement (kGy)	Total dose (kGy)	HAP fraction (Vol. %)	Collagen fraction (Vol. %)	Density (g/cm^3)	HAP strain rate ($\mu\text{e}/\text{min}$)	Fibrillar strain rate ($\mu\text{e}/\text{min}$)
Bone	A -95	27	24	672	43	37	2.35 ± 0.01	9.8 ± 1.0	-12 ± 2.4
	B -100	27	24	864	39	40	2.21 ± 0.02	14 ± 0.5	-35 ± 2.9
	C -108	27	24	816	41	39	2.08 ± 0.01	17 ± 0.6	-25 ± 2.2
	D -40	37	78	8034	42	37	2.21 ± 0.01	12 ± 1.7	-20 ± 3.3
	E -55	37	78	7332	40	38	2.15 ± 0.02	22 ± 1.1	-25 ± 2.8
	F -75	37	78	7722	43	37	2.21 ± 0.02	21 ± 1.3	-34 ± 3.5
	G -95	37	78	9360	41	38	2.08 ± 0.01	29 ± 1.5	-30 ± 5.9
	H -100	37	78	9204	40	38	2.19 ± 0.01	51 ± 2.4	-41 ± 9.8
	I -108	37	78	8814	38	39	2.13 ± 0.01	69 ± 2.3	-65 ± 9.1
	J -95	37	24	816	41	38	2.15 ± 0.01	17 ± 0.5	-23 ± 2.3
	K -100	37	24	840	40	38	2.10 ± 0.01	16 ± 0.7	-27 ± 1.7
	L -108	37	24	864	38	37	2.16 ± 0.03	33 ± 1.0	-40 ± 4.8
Dentin	M -90	27	24	576	40	30	1.99 ± 0.02	3.4 ± 0.4	-14 ± 0.8
	N -	27	24	720	39	32	1.97 ± 0.01	4.6 ± 0.4	-22 ± 1.1
	O -100	27	24	864	39	31	1.92 ± 0.01	16 ± 0.4	-11 ± 1.5
	P -90	37	24	864	38	30	1.93 ± 0.01	8.3 ± 0.3	-27 ± 1.2
	Q -	37	24	864	37	30	2.02 ± 0.02	7.3 ± 0.4	-35 ± 2.0
	R -95	37	24	888	42	30	1.98 ± 0.01	8.2 ± 0.3	-34 ± 1.4

density differences, which scatter at smaller angles to produce the SAXS pattern. SAXS thus measures the spacing between the HAP crystals. The change in SAXS spacing occurs due to the combined deformation of HAP and collagen and is taken as a measure of the fibrillar strain, as described in earlier works [34,35,39,41,51]. A pressed Ceria (CeO_2) powder disk is used as a standard to calibrate the WAXS patterns which are then used to determine the strains.

The method of HAP and fibrillar strain calculation has been described in detail in Ref. [32], and is summarized here. First, for HAP, the center of the peak of interest – (00.2) – in the diffraction patterns is determined, as a function of azimuthal angle, in terms of the radial distance from the center of the pattern. An invariant strain point, r^* , is determined as the point of intersection of the radius versus azimuth plots for a single peak at different applied stresses. Since, only single loads were used in this study a standard value of r^* calculated for bone and dentin in other studies was used. The radial position of the peak center at azimuthal angles of $90 \pm 5^\circ$ and $270 \pm 5^\circ$ (highlighted in the WAXS pattern in Fig. 1) is then referenced to the r^* value to determine the longitudinal HAP strain (i.e., strain along the macroscopic loading direction) at a particular load. A similar analysis is carried out to calculate the longitudinal fibrillar strains from the 3rd order scattering peak. The scattering rings are fit over azimuthal angles of $90 \pm 10^\circ$ and $270 \pm 10^\circ$ (highlighted in the SAXS pattern in Fig. 1) to calculate the longitudinal strains. In this case, however, the radius at zero stress is used as a reference to calculate the strain, because of incomplete rings which result from the pronounced longitudinal orientation of the collagen fibrils.

2.3.2. Peak orientation analysis

The intensity of the diffraction rings is normalized by the maximum intensity in the same ring, and plotted as a function of azimuth. Crystals which are slightly misoriented with respect to the longitudinal direction will diffract at their corresponding orientation angles. Peaks in intensity arise at the azimuths associated with preferred orientations. An example of the plot of intensity at all the azimuthal angles is shown in our earlier work [43]. The full-width at half-maximum (FWHM) of the (00.2) reflection intensity peaks (η -FWHM) is determined from the diffraction ring about $90 \pm 15^\circ$ and $270 \pm 15^\circ$ [43]. This peaks' η -FWHM is proportional to the degree of 001 HAP alignment with respect to the longitudinal/loading direction, with a lower value representing higher alignment.

2.4. Volume fraction determination

Thermogravimetric analysis (TGA) was performed on all samples after mechanical testing. Small specimens, weighing between 3 and 10 mg, were cut out from the compression samples using a low-speed diamond saw. These small pieces were maintained hydrated in PBS until the time of testing when they were blotted to remove the surface water, and loaded into alumina TGA pans. The bone samples were heated from room temperature to 680°C in air, at a rate of $10^\circ\text{C}/\text{min}$ and held at the maximum temperature for 10 min before cooling down. By measuring total weight loss between 25 and 200°C , as well as 200 – 500°C (according to Refs. [52,53]), the weight fractions of water, protein and HAP in the samples were determined. The dentin samples were heated using the same procedure. The weight fractions were then converted to volume fractions using densities of 3.2, 1.1 and $1\text{ g}/\text{cm}^3$ for HAP, collagen and water respectively [54]. Given the heterogeneity in biological samples from one location to the other [38,55], the volume fractions determined from these TGA samples may not be exactly representative of those in the diffracting volume, since they were obtained from an approximate location where the X-ray beam passed through the sample during the mechanical test. TGA measurements on two different volumes obtained from samples B and F were performed to estimate

reproducibility and show that the HAP volume fractions differ by an average of 0.7% between the two measurements.

3. Results

3.1. Volume fractions and density

Results for TGA-determined HAP content of bone and dentin are given in Table 1 for all samples, along with the applied stresses and doses at which they were tested. The average volume fractions of the HAP, collagen and water phases in bone are 41.0 ± 1.7 , 38.0 ± 1.0 and $21.0 \pm 1.7\%$ respectively. The average density of the bone samples is $2.17 \pm 0.08\text{ g}/\text{cm}^3$. Dentin samples show the same HAP content, but lower collagen and higher water content: the average volume fractions of HAP, collagen and water are 39.2 ± 1.7 , 30.5 ± 0.8 and $30.3 \pm 1.9\%$ respectively. As expected from the lower fraction of protein, the density is lower than for bone, with an average value of $1.97 \pm 0.05\text{ g}/\text{cm}^3$.

3.2. Creep

The HAP and fibrillar strains in the bone and dentin samples are shown as a function of time in Figs. 2–4 for all the stresses tested. The initial residual strain has been subtracted from the HAP strains plotted in Figs. 2a, b and 4 to eliminate the effect of variable initial strain, thus facilitating comparisons between samples. In both bone and dentin, the magnitude of the longitudinal compressive strains (accrued on initial application of the stress) decreases in the HAP phase and increases in the fibrillar phase with time, at all the stresses tested.

3.2.1. Creep plot shape

The shape of the strain vs. time curves (Figs. 2–4) can provide information as to the effect of time and applied stress on the load transfer from the collagen matrix to the HAP platelet. In the case of bones, the HAP strain vs. time curves (Figs. 2a, 4) show three distinct stages: (i) an initial slow decrease in the strain magnitude with time; (ii) a rapid decrease in strain magnitude; and (iii) a leveling out where the rate of decrease of the strain magnitude is slower, and can end in a plateau. For bone, all the cases show this three-stage behavior with the samples loaded at -40 , -55 , -75 and -108 MPa at 37°C (Fig. 2a), and -95 , -100 and -105 MPa at 37°C (Fig. 4) ending in plateaus. The final plateau occurs earlier (at about 80 min) in tests done at low applied stresses (-40 , -55 and -75 MPa), compared to those tests run at higher stress (i.e., 123 min for the test at -108 MPa in Fig. 2a). The plateau in Fig. 4 for the creep-unload samples G–I occurred sooner, at 40–52 min, than samples J–L tested at the same temperature but lower doses. Also, since stage (iii) begins earlier than the first unload in these samples (about 58 min), their strain rates can be compared with the creep-only samples. The duration of stage (i) also seems to be radiation-dose-dependent, lasting about 13 min for the high doses and lower stresses (-40 , -55 , and -75 MPa and 7488 kGy) in comparison to the 30–53 min seen in the samples tested at higher stresses and lower doses (compressive stress greater than or equal to -90 MPa , 800 kGy). In the samples tested at higher doses and higher stresses, i.e., samples G–I at 37°C , stage (i) lasts for about 8 min. The length of stage (i) in the samples measured at multiple temperatures also shows a temperature dependence, where stage (i) lasts for an average of 53 min in samples tested at 27°C (A–C) compared to 30 min for those at 37°C (J–L) tested at the same “lower doses.”

In dentin, the HAP strain vs. time plots do not exhibit a clear three stage shape (Fig. 2b). Most dentin samples, at both temperatures, exhibit a stage (i) of slow decrease in strain magnitude (for about 13 min at 27°C and 18 min at 37°C) before reaching a slightly steeper stage (ii) behavior. None of these samples have a stage (iii)

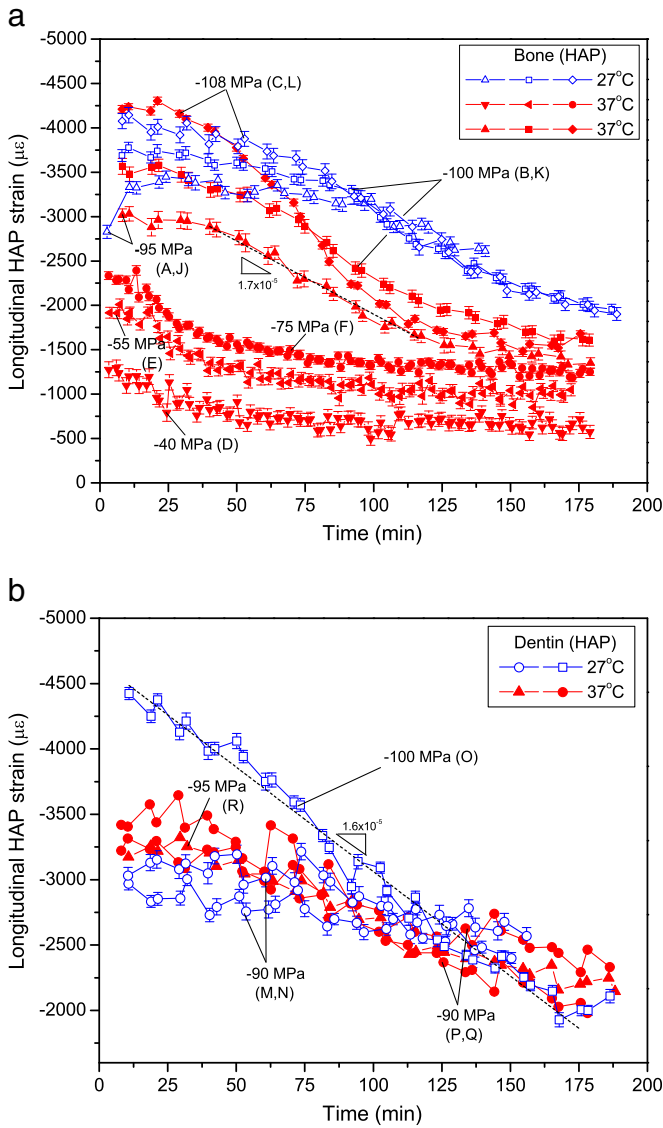


Fig. 2. Graph of longitudinal lattice strain in HAP vs. time at 27 and 37 °C in (a) bone (b) dentin.

or a plateau. Dentin sample O, tested at -100 MPa and 27 °C, shows no evidence of a stage (i) and instead has a very linear decrease in HAP strain magnitude with time.

The shape of the fibrillar strain curves is also different in bone and dentin. In bone, the magnitude of the fibrillar strains (Figs. 3a and 4) initially increases at a fast rate at both temperatures, and levels out towards the end of the 2–4 hour period of testing. The fibrillar strains in dentin (Fig. 3b) have a similar behavior at 37 °C, but the increase in magnitude is linear throughout the experiments at 27 °C.

3.2.2. Strain rates

Although the shapes of the curves are important to understanding the creep behavior of dentin and bone, one must also consider how the magnitude of the strain rate is affected by changes in temperature, applied stress, and radiation dose. These strain rates, corresponding to the rates of decrease in the HAP elastic strain magnitudes and increase in the fibrillar strain magnitudes as a function of time, are calculated by applying a best-fit linear regression to the data points in the strain vs. time plots of the two phases (Figs. 2–4). For samples where a

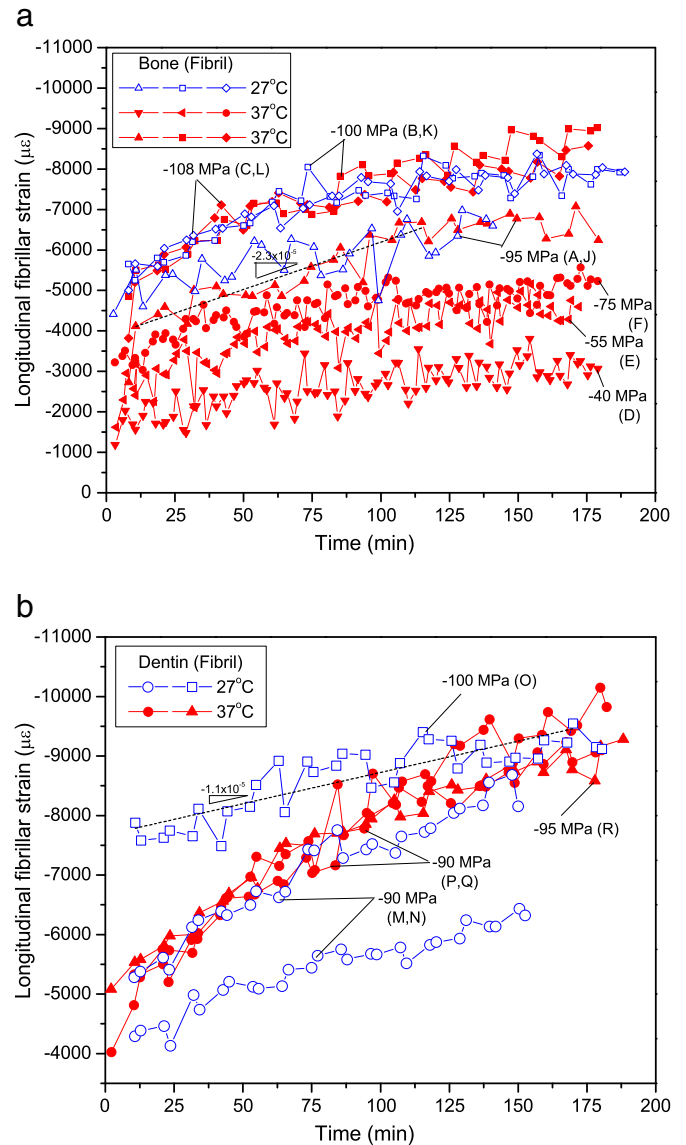


Fig. 3. Graph of longitudinal strain in collagen fibrils vs. time at 27 and 37 °C in (a) bone (b) dentin.

non-uniform increase (or decrease) exists, for example where stage (i) or (iii) behavior was present, the strain rates were calculated by taking a slope over the period of maximum increase (or decrease) corresponding to stage (ii).

In general the HAP strain rates are higher in bone than in dentin, whereas the fibrillar strain rates for the two materials are within error of each other (Table 1). The HAP strain rates in bone are found to generally increase with applied stress with $R^2 = 0.95$ at 27 °C (samples A–C, Fig. 5a) and for the samples measured at 37 °C, $R^2 = 0.59$ at high doses and low stresses (78 kGy/measurement, samples D–F in Fig. 5c), $R^2 = 0.99$ at high doses and high stresses (78 kGy/measurement, samples G–I in Fig. 5c) and $R^2 = 0.68$ at lower doses (24 kGy/measurement) and high stresses (samples J–L in Fig. 5a, c). As seen in Fig. 5a, these HAP strain rates, when compared at equal doses (24 kGy/measurement) and applied stresses (-95 , -100 , and -108 MPa), are greater at 37 °C compared to 27 °C. The samples tested at a higher dose (G–I) have a 2–3 times higher strain rate than the samples tested at a lower dose (J–L) at the same stresses and temperature, as seen in Fig. 5c. Also, the fibrillar strain rates in bone tend to increase with applied stress in a

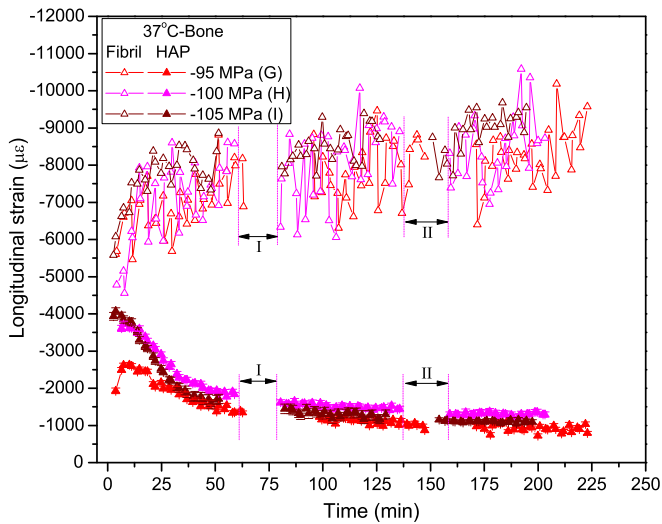


Fig. 4. Graph of longitudinal lattice strain in HAP vs. time at 37 °C for the creep/unload samples in bone. The unload/load segments are demarcated by short vertical dashed lines and their sequence is indicated by “I” and “II” in the figure.

non-linear fashion with $R^2=0.20$ at 27 °C (samples A–C, Fig. 5a) and linearly for measurements at 37 °C, with $R^2=0.91$ at 78 kGy/measurement and low stresses (samples D–F in Fig. 5c), $R^2=0.96$ at 78 kGy/measurement and high stresses (samples G–I in Fig. 5c) and $R^2=0.92$ at 24 kGy/measurement and high stresses (samples J–L in Fig. 5c). The fibrillar strain rate does not seem to be greatly affected by temperature, as there is no clear difference between the samples measured at 27 °C and 37 °C with stress. The fibrillar strain rates also do not show a clear dependence on the irradiation dose on the samples as seen in Fig. 5c.

In the dentin samples, the HAP strain rates at 27 °C are greater at –100 MPa (sample O) than at –90 MPa (samples M and N), and do not show any change with stress at 37 °C (Fig. 5b). The fibrillar strain rates also show no change with stress at 37 °C but decrease at 27 °C ($R^2=0.51$) (Table 1). The small number of different stresses measured for the dentin samples, makes it difficult to determine what effect the stress may have on the HAP or fibrillar strain rate of the dentin samples. Conversely, when comparing the four samples measured at –90 MPa (samples M and N at 27 °C and samples P and Q at 37 °C) as shown in Fig. 5b, it is apparent that the HAP and fibrillar elastic strain rates are significantly greater at 37 °C than at 27 °C.

3.2.3. Peak orientation

For all bone and dentin samples, the azimuthal full-width at half maximum, η -FWHM, of the (00.2) peak intensities about $\eta=90^\circ$ and 270° exhibits a slight increase with time before becoming constant. Fig. 6a shows representative examples of η -FWHM as a function of time for bone and dentin at –95 MPa and 37 °C. For this figure, the average η -FWHM is $57.9 \pm 0.5^\circ$ for dentin and $49.4 \pm 0.5^\circ$ for bone. The average η -FWHM over all the samples, irrespective of stress or temperature, is larger for dentin, $60.0 \pm 1.5^\circ$ than bone, $53.8 \pm 1.6^\circ$. As shown in Fig. 6b, the increase in the η -FWHM width shows a correlation with the applied stress in bone at 37 °C ($R^2=0.71$ for the low stresses at 78 kGy/measurement and $R^2=0.96$ for the high stresses at 24 kGy/measurement) but not at 27 °C ($R^2=0.22$). No correlation between η -FWHM and stress was found for the dentin samples. The increase in peak width does not show a correlation with temperature in either bone or dentin.

4. Discussion

4.1. Effect of irradiation

For all dentin and bone samples studied here, the overall creep behavior of the two phases was the same; the HAP strain decreased with creep time while the fibrillar strain increased. The opposite behavior is found in bone samples that underwent creep at a stress of –80 MPa at 37 °C and with minimal irradiation (2.8 kGy) [36]. In the low irradiation dose situation, stress is transferred from the viscoelastically deforming matrix to the reinforcing and elastic HAP, as expected for a composite with well bonded reinforcement [45,56,57]. The opposite trend seen here (HAP shedding load back to the matrix as the composite creeps) has been described in our previous experiments [35] for bone and dentin samples tested at –95 MPa and 37 °C and under high-dose irradiation conditions (637 kGy). In this earlier study [35], we proposed, as an explanation for this behavior, that the high doses of X-ray irradiation is accompanied by a delamination damage at the HAP–collagen interface. This interface is composed of electrostatic and Van der Waals type of interactions [58–62] making it relatively prone to damage; in particular the calcium-mediated electrostatic bonds can be broken due to collagen side-chain decarboxylation as a result of X-ray irradiation [63]. When coupled with continuous loading during creep, the interface becomes severely damaged and delaminates, thus changing the behavior of HAP from load accumulating in the case of an undamaged interface to load shedding [35]. This results in the observed decrease in the HAP elastic strains with creep. However, during loading, the collagen matrix is still continuously deforming due to a combination of elastic deformation through protein coiling and plastic deformation by collagen intermolecular sliding [64]. As a result, the fibrillar strains increase with creep. The effect of irradiation on the HAP rates can also be seen from the greater HAP strain rates in samples tested at a higher irradiation dose (G–I) as compared to those measured at lower doses (J–L) under equal stresses and temperature conditions (Fig. 5c). This suggests that as the irradiation dose increases, the HAP–collagen interface in the highly irradiated sample is more severely damaged and delaminates at a faster rate on loading, resulting in a more rapid decrease in the HAP strains as a function of time.

The shape of the HAP bone strain vs. time curves (Figs. 2a, 4) can be interpreted based on the relative rates of (a) damage (due to stress and radiation) which causes a release of HAP strain and (b) rate of load transfer to HAP from the collagen which increases the HAP strain. During stage (i), the HAP strain remains constant or decreases very slowly. During this early period, the interface is minimally damaged allowing the collagen to transfer some load; however, the high levels of stress and increasing dose during measurements both damage the interface, lowering the efficiency of load transfer. At a certain point in time, the combination of interfacial damage due to irradiation and high interfacial shear stresses causes the interfaces to fail allowing the collagen molecules to slide relative to each other as well as at the HAP–collagen interface. During this time, in stage (ii), the HAP is less constrained by the collagen and the initial elastic strain is released. In the final stage, stage (iii), the interfacial damage accumulation reaches equilibrium where no more strain can be dissipated in the HAP platelets. The HAP strain rate then slows and plateaus. This plateau is always at a non-zero value, likely due to the remaining bonding forces of water surface tension or Van der Waals interactions at the interface. It has also been theorized that irradiation induced collagen cross-linking may serve to constrain the HAP platelets slowing their relaxation [44].

In dentin, stage (ii) begins very soon after loading (Fig. 2b). This suggests that the HAP–collagen interface is damaged more rapidly in dentin than in bone. However, dentin exhibits a slower HAP strain rate than bone, implying that the rate of strain loss in the HAP is not

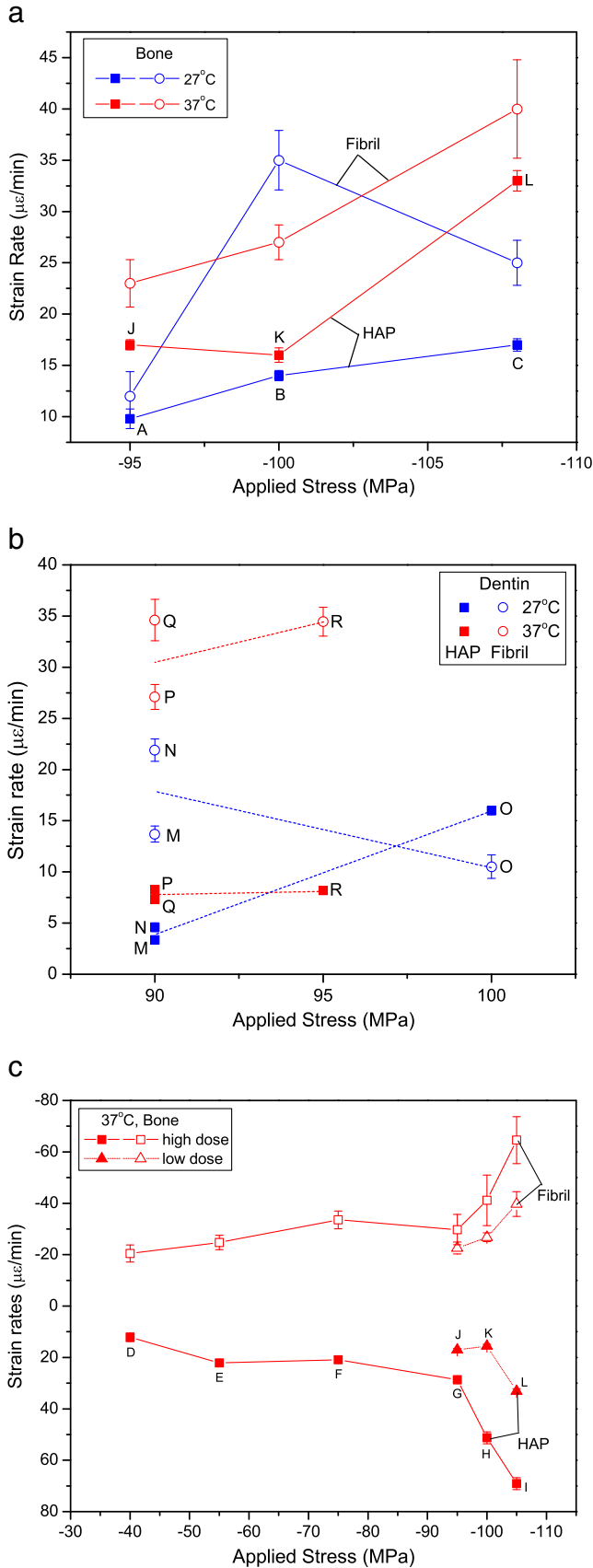


Fig. 5. Plot of HAP and fibril strain rates at different temperatures for matching stresses in (a) bone and (b) dentin. (c) HAP (closed symbols) and fibrillar (open symbols) strain rates as a function of applied stress for bone measured at 37 °C at the same irradiation dose level.

solely controlled by interfacial damage but also by structural or organizational parameters [2,40,65]. The internal structure of dentin is such that the collagen fibrils are distributed with their axis tangential to the circumference of the tubules which themselves radiate from the pulp cavity to the dentino-enamel junction in planes perpendicular to the applied stress [66]. The internal structure of bone, on the other hand, is more textured, with the collagen fibrils being mostly oriented along the bone long axis (direction of compression) [67]. This difference in fibril orientation can be seen in the higher 00.2 peak η -FWHM found in dentin than in bone (Fig. 6a), suggesting a broader distribution of platelet orientations. The significant orientation spreads prior to deformation in both dentin and bone make detection of changes challenging; nonetheless some trends can be observed as described below. This less aligned arrangement of the collagen fibrils within the dentin will result in greater geometric hindrances on the collagen intermolecular sliding compared to that in bone where the fibrils are mostly aligned along the same direction. With limitations on the sliding of collagen molecules, the interfacial shear strain will be restricted thus preserving the interface and lowering the HAP strain rate. The similarity in the fibrillar strain rates between the bone and the dentin indicates that the collagen plastic deformation, which is controlled by collagen intermolecular sliding as seen in tendon [64], is reduced in similar amounts by load transfer to the HAP platelets, as expected given the similar HAP fractions in bone and dentin.

4.2. Effect of stress

In general, the magnitude of the HAP strain rate increases with increasing applied stress in bone at both 27 and 37 °C and at both irradiation doses per measurement (Fig. 5a, c). The magnitude of the fibrillar strain rates in bone also increases with applied stress. Most materials which exhibit stress-relaxation behaviors show an increased macroscopic deformation rate with increased applied load during creep [68]. Therefore, it is expected that that strain rate of the fibril, which represents the HAP–collagen composite smallest unit and composes the bulk of bone and dentin, also increases with applied stress. The increase in the magnitude of the HAP strain rate with increasing load indicates that the extent of interfacial damage is not purely dependent on radiation damage but also on the applied load. This further supports the hypothesis that the interfacial damage is caused by a combination of chemical debonding due to irradiation damage and mechanical debonding due to interfacial shear stresses. As the magnitude of the compressive applied load grows, the interfacial stresses increase causing the bonds to break more rapidly, thus releasing the stored elastic strain in the HAP more quickly. As can be seen in Fig. 5c, identical fibrillar strain rates were reached at –75 MPa with 78 kGy/measurement and at –108 MPa with 24 kGy/measurement and HAP strain rates at –55 and –75 MPa with 78 kGy/measurement were higher than the HAP strain rates at –95 and –100 with 24 kGy/measurement. This supports the hypothesis that higher irradiation doses lead to higher levels of interfacial damage [35]. Even though the applied stress is 30–50% greater at the higher stresses, the strain rate is approximately the same, possibly because the higher irradiation dose has chemically damaged the interface in the sample tested at the lower stresses more extensively.

As mentioned above, both the HAP and the fibrillar strain rates do not always exhibit linear behavior with applied stress. With the limited number of samples and the small sampling volumes used here, sample inhomogeneities can have a significant effect. Mineral and protein content in the bone and dentin samples can have an important effect on the load transfer and creep behavior. There is a negative correlation between the HAP strain rate and the HAP content ($R = -0.2$), and positive correlation between HAP strain rate and protein content ($R = 0.53$) in all the samples (bone and dentin)

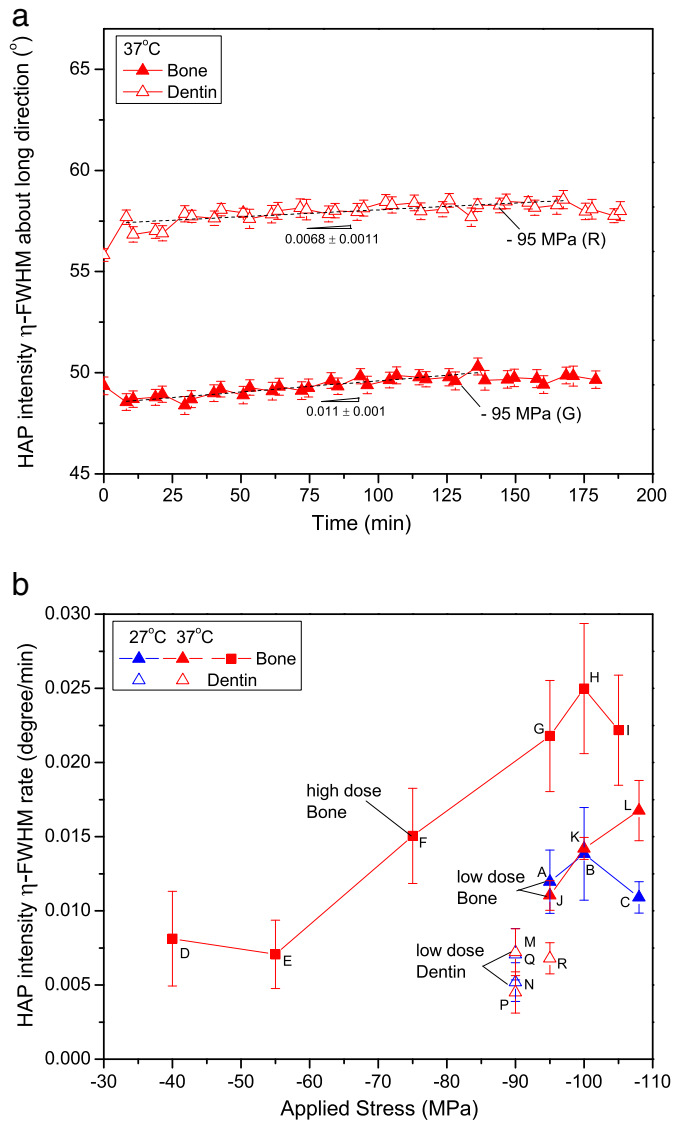


Fig. 6. (a) Plot of HAP 00.2 intensity peak FWHM as a function of time for -95 MPa at 37 °C in bone (sample G) and dentin (sample R). (b) Plot of the 00.2 Intensity peak FWHM rate as a function of stress at 27 °C (blue) and 37 °C (red) for bone (closed symbols) and dentin (open symbols).

which could possibly account for the non-linearity. An increase in the number of HAP platelets per unit volume would result in the applied load being distributed over more reinforcements. This means that each individual platelet carries less stress (or elastic strain), and thus the HAP–collagen interfacial stress decreases, together with the HAP strain rate. A higher HAP content also decreases the fibril strain rate ($R = -0.40$ for all the samples in the present work) by stiffening and strengthening the composite and inhibiting collagen intermolecular sliding. Similarly, higher collagen content will increase the compliance of the material, resulting in higher shear stresses due to intermolecular sliding within the collagen network as well as collagen molecular sliding at the HAP–collagen interface. This will cause an increase in the HAP strain rate.

The dentin HAP strain rates show no clear trend with applied stress (Fig. 5b). The limited number ($N = 2$ at each temperature) of different applied stresses and the small differences in the magnitude of these applied stresses prevent the determination of a trend. However, the pairs of repeated measurements at -90 MPa for both 27 °C and 37 °C illustrate the repeatability of the measurements. At both temperatures, the difference between the two measured samples was ~ 1 $\mu\epsilon$ /min.

The η -FWHM of the 00.2 peaks at $90 \pm 15^\circ$ and $270 \pm 15^\circ$ increases slightly with time for all the samples of bone and dentin tested here (Fig. 6a), suggesting the HAP crystals are tilting away from their original longitudinal alignment as creep strain accumulates. This behavior is as expected for a fiber reinforced composite, with longitudinally aligned fibers in a creeping matrix, deforming under compression, where the fibers are deflected away from the loading axis with increasing creep time [69–71]. In bone, the η -FWHM increases with stress (Fig. 6b) at 37 °C for both irradiation and stress conditions, but shows no trend at 27 °C. The η -FWHM in dentin samples do not show stress dependence at any temperature (Fig. 6b). For the dentin samples as well as the bone samples, the small number of samples and stresses ($N = 3$) make it difficult to detect a trend. However, an increase in η -FWHM with stress in bone at 37 °C is expected, considering the fact that a greater stress imposed on fibers would cause more tilting.

4.3. Effect of temperature

In both materials, the magnitude of the HAP strain rates increases with increasing temperature, from 27 °C to 37 °C, as shown in Fig. 5a in bone, and 5b in dentin. The magnitude of the fibrillar strain rate also increases with temperature for bone and dentin, except in bone at -100 MPa. This suggests that the rate of collagen sliding, which results in increased deformation and interfacial damage, increases with temperature. This is supported by the fact that the strength of the hydrogen bonds, electrostatic interactions and hydrophobic interactions that hold the collagen molecules together [6,72] decrease with an increase in temperature [6,72,73], increasing the collagen compliance, thus facilitating collagen sliding. The outliers at -100 MPa in bone are probably a result of differences in the composition or structure between the two sampled volumes. Although the macroscopic density and HAP content is not different between the two samples (B and K), the X-ray diffraction volume is comparatively small and is subjected to the large intra-sample variations present in biological hard tissue, as discussed for dentin in Ref. [43].

In bone, the shorter stage (i) in HAP at 37 °C compared to 27 °C suggests that the damage rate is higher at the higher temperature. The shape of the strain versus time curves in dentin, on the other hand, does not show a change with temperature (Fig. 2b). It is expected that damage would set in sooner and occur to a larger extent at the higher temperature (37 °C) because, beyond the increased collagen compliance, the strength of the hydrogen bonds and charged interactions at the HAP–collagen interface also become weaker [73,74] with increased temperature. The relatively weaker interface allows a faster rate of delamination as seen from an increase in the HAP strain rates. The fibrillar strain rates also increase with temperature due to the overall increase in the compliance of the composite at a higher temperature. Thus, these data confirm that the deformation of bone and dentin is temperature-dependent, and that mechanical properties of these biological materials should be determined at body temperature to achieve an accurate understanding of their *in vivo* performance.

The increase in η -FWHM with time does not show any correlation with temperature in either bone (Fig. 6a) or dentin. This is contrary to what one would expect since the relatively weaker bonds at 37 °C would permit greater sliding between the collagen molecules [64,75,76] than at 27 °C, allowing for a greater tendency for misalignment. It is unclear why such behavior is not seen but it is possible that the tilting behavior is not only controlled by the collagen compliance but also by other structural parameters such as mineral content in the fibril, fibril orientation, or location within the larger hierarchical framework.

5. Conclusions

Synchrotron X-ray diffraction is used to study the strain evolution in the phases of highly irradiated bone and dentin as a function of

applied compressive stresses, ambient (27 °C) and body temperature (37 °C), and irradiation dose. The strain evolution during creep (decreasing for HAP and increasing for fibrillar strain) is consistent with the hypothesis that delamination takes place at the HAP–collagen interface, at all stresses and temperatures tested here. The temporal evolution of HAP elastic strains in bone is complex under creep but follows a common pattern: an initial stage of slow strain decrease is followed by a rapidly decreasing stage, finally ending in a strain plateau. The extent of these three stages depends on the applied stress, temperature and accumulated radiation dose in bone. The HAP elastic strains in dentin, by contrast, decrease in a more linear fashion, indicating earlier onset of interfacial damage. In both bone and dentin, the HAP platelets tilt away from the loading direction as creep proceeds.

The HAP elastic strain rates are compared directly between bone and dentin; the greater strain rates in bone than those in dentin are likely due the differing hierarchical structures in the two materials. The magnitude of the HAP and fibrillar strain rates in bone increase with applied stress indicating greater damage. HAP platelet tilting in bone also increases with increased stress at higher temperatures. There were too few dentin samples and measured stresses to realistically determine the effect of stress on the dentin creep behavior.

The magnitude of the HAP strain rate is greater at body temperature (37 °C) than room temperature (27 °C) at the same applied stress in both bone and dentin. This is probably because bonds at the collagen–collagen and HAP–collagen interfaces become weaker with increasing temperature, promoting more sliding and delamination. This confirms prior studies indicating that testing at body temperature, rather than ambient temperature, is necessary to appropriately capture the *in vivo* behavior of bone and teeth.

Acknowledgments

The authors thank Prof. L. Catherine Brinson (NU), Dr. S.R. Stock (NU), Mr. Fang Yuan (NU) and Dr. Dean R. Haefner (APS) for numerous useful discussions throughout this work. They also acknowledge Dr. Yu-chen Karen Chen-Wiegart (NU) and Mr. Fang Yuan (NU) for their help with the experiments at the APS. This research was performed at station 1-ID of XOR-APS. Use of the Advanced Photon Source was supported by the U.S. Department of Energy, Office of Science, Office of Basic Energy Sciences, under Contract No. DE-AC02-06CH11357. Partial funding was provided to A.C.D.B. by a National Defense Science and Engineering Graduate Fellowship from the Department of Defense and by a Graduate Fellowship from the National Science Foundation.

References

- [1] M.J. Olszta, X. Cheng, S.S. Jee, R. Kumar, Y.-Y. Kim, M.J. Kaufman, E.P. Douglas, L.B. Gower, *Mater. Sci. Eng.*, R 58 (2007).
- [2] M.A. Meyers, P.-Y. Chen, A.Y.-M. Lin, Y. Seki, *Prog. Mater. Sci.* 53 (2008) 1–206.
- [3] D.T. Reilly, A.H. Burstein, *J. Biomech.* 8 (1975) 393–405.
- [4] X.N. Dong, X.E. Guo, *J. Biomech.* 37 (2004) 1281–1287.
- [5] R. Shahar, P. Zaslansky, M. Barak, A.A. Friesem, J.D. Currey, S. Weiner, *J. Biomech.* 40 (2007) 252–264.
- [6] S.S. Mehta, O.K. Oz, P.P. Antich, *J. Bone Miner. Res.* 13 (1998) 114–121.
- [7] R.G. Craig, F.A. Peyton, *J. Dent. Res.* 37 (1958) 710–719.
- [8] J.H. Kinney, J.R. Gladden, G.W. Marshall, S.J. Marshall, J.H. So, J.D. Maynard, *J. Biomech.* 37 (2004) 437–441.
- [9] F.A. Peyton, D.B. Mahler, B. Hershenov, *J. Dent. Res.* 31 (1952) 366–370.
- [10] R.K. Nalla, R.P. Pollack, J.L. Katz, *Arch. Oral Biol.* 15 (1970) 787–796, (IN717).
- [11] H. Peterlik, P. Roschger, K. Klaushofer, P. Fratzl, *Nat. Mater.* 5 (2006) 52–55.
- [12] M.J. Buehler, *Nanotechnology* 18 (2007).
- [13] R.K. Nalla, J.H. Kinney, R.O. Ritchie, *Nat. Mater.* 2 (2003) 164–168.
- [14] H.S. Gupta, W. Wagermaier, A. Zickler, J. Hartmann, S.S. Funari, P. Roschger, H.D. Wagner, P. Fratzl, *Int. J. Fract.* 139 (2006) 425–436.
- [15] A.C. Deymier-Black, F. Yuan, A. Singhal, J.D. Almer, L.C. Brinson, D.C. Dunand, *J. Mech. Behav. Biomed. Mater.* (under review).
- [16] O.M. El Mowafy, D.C. Watts, *J. Dent. Res.* 65 (1986) 677–681.
- [17] B. Kahler, M.V. Swain, A. Moule, *J. Biomech.* 36 (2003) 229–237.
- [18] J.J. Kruczic, R.K. Nalla, J.H. Kinney, R.O. Ritchie, *Biomaterials* 24 (2003) 5209–5221.
- [19] S.T. Rasmussen, R.E. Patchin, D.B. Scott, A.H. Heuer, *J. Dent. Res.* 55 (1976) 154–164.
- [20] S.T. Rasmussen, R.E. Patchin, *J. Dent. Res.* 63 (1984) 1362–1368.

- [21] K.H. Bridwell, *Spine* 24 (1999) 2607–2616.
- [22] E.A. Bonfils-Roberts, *Chest* 61 (1972) 469–474.
- [23] R.A. Hocevar, *Am. J. Orthod. Dentofac. Orthop.* 80 (1981) 457–477.
- [24] C.M. Rinnac, A.A. Petko, T.J. Santner, T.W. Wright, *J. Biomech.* 26 (1993).
- [25] J. Jantarat, J.E.A. Palamara, C. Lindner, H.H. Messer, *Dent. Mater.* 18 (2002) 486–493.
- [26] M.L. Young, J. DeFouw, J.D. Almer, D.C. Dunand, *Acta Mater.* 55 (2007) 3467–3478.
- [27] M.L. Young, J.D. Almer, M.R. Daymond, D.R. Haefner, D.C. Dunand, *Acta Mater.* 55 (2007) 1999–2011.
- [28] T.E. Wilkes, B.J. Harder, J.D. Almer, K.T. Faber, *Acta Mater.* 57 (2009) 6234–6242.
- [29] S. Roy, J. Gibmeier, A. Wanner, *Adv. Eng. Mater.* 11 (2009) 471–477.
- [30] M.L. Young, R. Rao, J.D. Almer, D.R. Haefner, J.A. Lewis, D.C. Dunand, *Acta Mater.* 57 (2009) 2362–2375.
- [31] R. Akhtar, M.R. Daymond, J.D. Almer, P.M. Mummery, *Acta Biomater.* 4 (2008) 1677–1687.
- [32] J.D. Almer, S.R. Stock, *J. Struct. Biol.* 152 (2005) 14–27.
- [33] J.D. Almer, S.R. Stock, *J. Struct. Biol.* 157 (2007) 365–370.
- [34] H.S. Gupta, J. Seto, W. Wagermaier, P. Zaslansky, P. Boesecke, P. Fratzl, *PNAS* 103 (2006) 17741–17746.
- [35] A. Deymier-Black, F. Yuan, A. Singhal, J.D. Almer, D.C. Dunand, *Bone* (under review).
- [36] A.C. Deymier-Black, F. Yuan, A. Singhal, J.D. Almer, L.C. Brinson, D.C. Dunand, *Acta Biomater.* 8 (2011) 253–261.
- [37] R. Akhtar, M.R. Daymond, J.D. Almer, P.M. Mummery, *Acta Biomater.* 7 (2011) 716–723.
- [38] A. Singhal, F.Y. Stuart, R. Stock, J.D. Almer, L. Catherine Brinson, D.C. Dunand, *Adv. Eng. Mater.* (2012), <http://dx.doi.org/10.1002/adem.201200204>.
- [39] A. Singhal, A. Deymier-Black, J.D. Almer, D.C. Dunand, *J. Mech. Behav. Biomed. Mater.* 4 (2011) 1774–1786.
- [40] A.C. Deymier-Black, J.D. Almer, S.R. Stock, D.R. Haefner, D.C. Dunand, *Acta Biomater.* 6 (2010) 2172–2180.
- [41] A.C. Deymier-Black, J.D. Almer, D.R. Haefner, D.C. Dunand, *Mater. Sci. Eng., C* 31 (2011) 1423–1428.
- [42] J.D. Almer, S.R. Stock, *J. Biomech.* 43 (2010) 2294–2300.
- [43] A.C. Deymier-Black, S.R. Stock, J.D. Almer, D.C. Dunand, *J. Mech. Behav. Biomed. Mater.* 5 (2012) 71–81.
- [44] A.C. Deymier-Black, A. Singhal, J.D. Almer, D.C. Dunand, *Acta Biomater.* 9 (2) (2013) 5305–5312.
- [45] M.R. Daymond, C. Lund, M.A.M. Bourke, D.C. Dunand, *Metall. Mater. Trans. A* 30A (1999).
- [46] D.R. Carter, W.C. Hayes, *J. Bone Joint Surg. Br.* 59 (1977).
- [47] Y.N. Yeni, C.U. Brown, T.L. Norman, *Bone* 22 (1998).
- [48] S.C. Cowin, *Bone Mechanics*, CTC Press, Boca Raton, Fla., 1989.
- [49] D.B. Burr, C. Milgrom, D. Fyhrie, M. Forwood, M. Nyska, A. Finestone, S. Hoshaw, E. Saia, A. Simkin, *Bone* 18 (1996) 405–410.
- [50] J.H. Hubbell, S.M. Seltzer, in: *National Institute of Standards and Technology, Gaithersburg, MD, 2004*, (<http://physics.nist.gov/xaamdi>).
- [51] H.S. Gupta, W. Wagermaier, G.A. Zickler, D.R.-B. Aroush, S.S. Funari, P. Roschger, H.D. Wagner, P. Fratzl, *Nano Lett.* 5 (2005).
- [52] L.F. Lozano, M.A. Pena-Rico, A. Heredia, J. Octalan-Flores, A. Gomez-Cortes, R. Velazquez, I.A. Belio, L. Bucio, *J. Mater. Sci.* 38 (2003) 4777–4782.
- [53] L.D. Mkukuma, C.T. Imrie, J.M.S. Skakle, D.W.L. Hukins, R.M. Aspden, *Ann. Rheum. Dis.* 64 (2005).
- [54] R.B. Martin, D.B. Burr, N.A. Sharkey, *Skeletal Tissue Mechanics*, 1998.
- [55] A. Singhal, S.R. Stock, J.D. Almer, D.C. Dunand, *Biomech. Model. Mechanobiol.* (under review).
- [56] A. Madgwick, T. Mori, P.J. Withers, *Mater. Sci. Eng., A* 333 (2002) 232–238.
- [57] H.M.A. Winand, A.F. Whitehouse, P.J. Withers, *Mater. Sci. Eng. A* 284 (2000) 103–113.
- [58] E.R. Wise, S. Maltsev, M.E. Davies, M.J. Duer, C. Jaeger, N. Loveridge, R.C. Murray, D.G. Reid, *Chem. Mater.* 19 (2007) 5055–5057.
- [59] J.D. Currey, *Nat. Mater.* 414 (2001) 699.
- [60] G.E. Fantner, T. Hassenkam, J.H. Kindt, J.C. Weaver, H. Birkedal, L. Pechenik, J.A. Curtoni, G.G. Cidade, G.D. Stucky, D.E. Morse, P.K. Hansma, *Nat. Mater.* 4 (2005) 612–616.
- [61] L.H. He, M.V. Swain, *Biomaterials* 28 (2007) 4512–4520.
- [62] D.G. Reid, M.J. Duer, R.C. Murray, E.R. Wise, *Chem. Mater.* 20 (2008) 3549–3550.
- [63] W. Hubner, A. Blume, R. Pushnjakova, Y. Dekhtyar, H.-J. Hein, *Int. J. Artif. Organs* 28 (2005) 66–73.
- [64] N. Sasaki, S. Odajima, *J. Biomech.* 29 (1996) 1131–1136.
- [65] P.-Y. Chen, A.Y.M. Lin, Y.-S. Lin, Y. Seki, A.G. Stokes, J. Peyras, E.A. Olevsky, M.A. Meyers, J. McKittrick, *J. Mech. Behav. Biomed. Mater.* 1 (2008) 208–226.
- [66] L. Bozec, J.D. Groot, M. Odlyha, B. Nicholls, S. Nesbitt, A. Flanagan, *Ultramicroscopy* 105 (2005) 79–89.
- [67] S. Weiner, H.D. Wagner, *Annu. Rev. Mater. Sci.* 28 (1998) 28.
- [68] W. Grellmann, S. Seidler, *Polymer Testing*, Carl Hanser Verlag, Munich, 2007.
- [69] T. Venkatesh, D. Dunand, *Metall. Mater. Trans. A* 32 (2001) 183–196.
- [70] J. Liu, L.H. Qi, J.T. Guan, Y.Q. Ma, J.M. Zhou, *Mater. Sci. Eng. A* 531 (2012) 164–170.
- [71] L. Geng, A.B. Li, Q.Y. Meng, *Mater. Sci. Eng. A* 386 (2004) 212–221.
- [72] D.J.S. Hulmes, A. Miller, D.A.D. Parry, K.A. Piez, J. Woodhead-Galloway, *J. Mol. Biol.* 79 (1973) 137–148.
- [73] J. Yan, K.B. Clifton, J.J.M. Jr., L.A. Gower, *J. Biomech.* 40 (2007).
- [74] W.R. Walsh, N. Guzelsu, *Biomaterials* 15 (1994) 137–145.
- [75] E. Mosler, W. Folkhard, E. Knorz, H. Nemetschek-Gansler, T. Nemetschek, M.H.J. Koch, *J. Mol. Biol.* 182 (1985) 589–596.
- [76] W. Folkhard, E. Mosler, W. Geercken, E. Knorz, H. Nemetschek-Gansler, T. Nemetschek, M.H.J. Koch, *Int. J. Biol. Macromol.* 9 (1987) 169–175.